Contrast enhanced computed tomography for real-time quantification of glycosaminoglycans in cartilage tissue engineered constructs

Garcia, João P.; Longoni, Alessia ; Gawlitta, Debby ; Rosenberg, Antoine J.W.P. ; Grinstaff, Mark W. ; Töyräs, Juha ; Weinans, Harrie; Creemers, Laura B.; Pouran, Behdad

DOI
10.1016/j.actbio.2019.09.014

Publication date
2019

Document Version
Final published version

Published in
Acta Biomaterialia

Acta Biomaterialia 100 (2019) 202–212

Contents lists available at ScienceDirect

Acta Biomaterialia

journal homepage: www.elsevier.com/locate/actbio

Full length article

Contrast enhanced computed tomography for real-time quantification of glycosaminoglycans in cartilage tissue engineered constructs

João P. Garcia[a], Alessia Longoni[b], Debby Gawlitta[b], Antoine J.W.P. Rosenberg[b], Mark W. Grinstaff[c], Juha Töyräs[d,e,f], Harrie Weinans[a,g], Laura B. Creemers[a], Behdad Pouran[a,g,*]

[a] Department of Orthopedics, University Medical Centre Utrecht, Heidelberglaan 100, 3508 GA Utrecht, The Netherlands
[b] Department of Oral and Maxillofacial Surgery & Special Dental Care, University Medical Center Utrecht, Heidelberglaan 100, 3508 GA Utrecht, The Netherlands
[c] Departments of Chemistry and Biomedical Engineering, Boston University, MA 02215, Boston, USA
[d] Department of Applied Physics, University of Eastern Finland, Yliopistonranta 1F, 70210 Kuopio, Finland
[e] Diagnostic Imaging Centre, Kuopio University Hospital, Puijonlaaksontie 2, 70210 Kuopio, Finland
[f] School of Information Technology and Electrical Engineering, The University of Queensland, St Lucia Campus, QLD 4072, Brisbane, Australia
[g] Department of Biomechanical Engineering, Delft University of Technology, Mekelweg 2, 2628 CD Delft, The Netherlands

ARTICLE INFO

Article history:
Received 3 April 2019
Revised 6 September 2019
Accepted 11 September 2019
Available online 30 September 2019

Keywords:
Tissue engineering
Cartilage regeneration
Glycosaminoglycans
3D imaging
Computed tomography

ABSTRACT

Tissue engineering and regenerative medicine are two therapeutic strategies to treat, and to potentially cure, diseases affecting cartilaginous tissues, such as osteoarthritis and cartilage defects. Insights into the processes occurring during regeneration are essential to steer and inform development of the envisaged regenerative strategy, however tools are needed for longitudinal and quantitative monitoring of cartilage matrix components. In this study, we introduce a contrast-enhanced computed tomography (CECT)-based method using a cationic iodinated contrast agent (CA4+) for longitudinal quantification of glycosaminoglycans (GAG) in cartilage-engineered constructs. CA4+ concentration and scanning protocols were first optimized to ensure no cytotoxicity and a facile procedure with minimal radiation dose. Chondrocyte and mesenchymal stem cell pellets, containing different GAG content were generated and exposed to CA4+. The CA4+ content in the pellets, as determined by micro computed tomography, was plotted against GAG content, as measured by 1,9-dimethylmethylene blue analysis, and showed a high linear correlation. The established equation was used for longitudinal measurements of GAG content over 28 days of pellet culture. Importantly, this method did not adversely affect cell viability or chondrogenesis. Additionally, the CA4+ distribution accurately matched safranin-O staining on histological sections. Hence, we show proof-of-concept for the application of CECT, utilizing a positively charged contrast agent, for longitudinal and quantitative imaging of GAG distribution in cartilage tissue-engineered constructs.

Statement of Significance: Tissue engineering and regenerative medicine are promising therapeutic strategies for different joint pathologies such as cartilage defects or osteoarthritis. Currently, *in vitro* assessment on the quality and composition of the engineered cartilage mainly relies on destructive methods. Therefore, there is a need for the development of techniques that allow for longitudinal and quantitative imaging and monitoring of cartilage-engineered constructs. This work harnesses the electrostatic interactions between the negatively-charged glycosaminoglycans (GAGs) and a positively-charged contrast agent for longitudinal and non-destructive quantification of GAGs, providing valuable insight on GAG development and distribution in cartilage engineered constructs. Such technique can advance the development of regenerative strategies, not only by allowing continuous monitoring but also by serving as a pre-implantation screening tool.

* Corresponding author at: University Medical Centre Utrecht, Heidelberglaan 100, 3508 GA Utrecht, The Netherlands.
E-mail address: b.pouran@umcutrecht.nl (B. Pouran).

https://doi.org/10.1016/j.actbio.2019.09.014
1742-7061/

1. Introduction

Joint disorders are a major cause of morbidity and disability worldwide, and represent both significant healthcare and socio-economical burdens [1]. Osteoarthritis (OA) and joint trauma, which adversely affect articular cartilage, ultimately lead to its degradation over time [2,3]. The extracellular matrix (ECM) of cartilage is mainly composed of proteoglycans, collagen II, and water [2]. The pathogenesis of degeneration is still poorly understood, however degradation is accompanied by breakdown of proteoglycans, which inherently induces a reduction in the mechanical properties and poorer functional performance of the tissue [2]. Currently, disease modifying therapies remain unavailable for OA and treatments are limited to pain relief and palliative care at early stages, and joint prosthesis at the end-stage [2,4]. Hence, there is a need for new treatment modalities that promote tissue repair and regeneration. In this context, tissue engineering and regenerative medicine are of interest as therapeutic approaches [4,5], which employ the use of cells, biomaterial scaffolds, and/or stimulatory factors to ultimately produce cartilaginous-like tissue [5]. Currently, most of the available techniques to assess the effects of these factors on matrix production and tissue quality are destructive. Usually, engineered-tissues are harvested at mid or endpoints and subjected to biochemical assays such as the 1,9-dimethylmethylene blue (DMMB) and hydroxyproline assays for quantification of total glycosaminoglycans (GAGs) and collagen content, respectively [6,7]. In addition, constructs can be processed for histology and immunohistochemistry (IHC), which only provide a two-dimensional and qualitative assessment of matrix components and tissue quality [8,9]. However, the detailed understanding of the regeneration process over time is crucial for achieving full regenerative potency *in vitro* and *in vivo*. Therefore, it is of significant importance to develop non-invasive and non-destructive imaging techniques for real-time, three-dimensional (3D), and quantitative monitoring of cartilage tissue-engineered constructs. Such techniques will enable monitoring of *in vitro* regeneration over time, evaluation of ECM components, optimization of chondrogenic activity, and, ultimately, screening to identify the best performing tissue constructs before implantation.

Efforts are ongoing to develop such tools and techniques. For example, ultrasound was used as a standalone procedure or in combination with fluorescence techniques to assess both matrix composition and mechanical properties in cartilage tissue-engineered constructs [10–14]. More recently, a set of reporter genes was described for transfection of MSCs as a monitoring tool for real-time characterization of the chondrogenic differentiation process [15]. Also dielectric impedance spectroscopy was proposed as a label-free and non-destructive method to evaluate cellular viability and survival during and after biofabrication processes [16]. Despite these recent advances, most of the described techniques are qualitative, do not quantify ECM components, or lack the resolution to assess the 3D distribution of the matrix components.

Contrast-enhanced computed tomographic (CECT) imaging is a rapid and readily available imaging modality used to study many different tissues [17], namely tissues with low X-ray attenuation to include articular cartilage [18–22], meniscus [23–25], intervertebral disc [26–28], and xiphoid cartilage [29]. Due to the compositional differences among these tissues, contrast agent diffusion and flux will vary [20,24]. While GAGs are mainly responsible for electrostatic interactions, collagen fibers will drive steric hindrance [24]. CECT provides unique high-resolution 3D information and quantification on composition and distribution of crucial constituents within articular cartilage. Charge-driven transport of negatively or positively charged iodinated contrast agents (*i.e.*, ioxaglate and CA4+, respectively) provides more efficient imaging of GAGs with greater sensitivity [30–33]. Due to the anionic fixed charge of cartilage ECM, anionic contrast agents inversely correlate with GAG content, while positively-charged contrast agents display a positive correlation with GAG content with considerably higher sensitivity [18,20,28,30,34–38]. Hence, we hypothesize that CA4+-based CECT will allow for longitudinal imaging and GAG quantification in cartilage tissue-engineered constructs. In this work, we propose a CECT-based approach as a high-resolution 3D "histology" technique for real-time spatiotemporal quantification of total GAG content in tissue-engineered constructs, which potentially replaces the currently available destructive assays.

2. Materials and methods

2.1. Cell isolation and culture

Human articular chondrocytes (ACs) were isolated from articular cartilage from patients with OA undergoing total knee arthroplasty. The anonymous use of redundant tissue for research purposes is part of the standard treatment agreement with patients in the University Medical Center Utrecht and was carried out under protocol n° 15–092 of the UMCU's Review Board of the BioBank. Chondrocytes were isolated by mincing and subsequently digesting the cartilage overnight at 37 °C in Dulbecco's Modified Eagle's Medium Glutamax (31966, DMEM, Gibco) supplemented with 0.15% (w/v) type II collagenase (CLS-2, Worthington Biochemical Corporation), 10% (v/v) Fetal Bovine Serum (FBS, S14068S1810, Biowest), and 100 U/mL penicillin and 100 mg/ml streptomycin (15140122, Gibco).

Undigested debris was removed using a 70 μm cell strainer followed by a PBS wash. Subsequently, cells were plated and grown in a humidified incubator at 37 °C and 5% CO_2 with expansion medium consisting of DMEM supplemented with 10% FBS, 0.2 mM ascorbic-2-phosphate (ASAP, A8960, Sigma-Aldrich), 100 U/mL penicillin, 100 mg/ml streptomycin and 10 ng/mL basic fibroblast growth factor (bFGF, 233-FB; R&D Systems). Medium was renewed every 3 days. Cells were expanded until passage one, frozen, stored, and subsequently thawed and used for experiments at passage 2.

Human mesenchymal stem cells (MSCs) were isolated from the bone marrow aspirate of a 20-year old female patient. The aspirate was taken after informed consent, according to a protocol approved by the local Medical Ethics Committee (TCBio-08-001-K University Medical Centre Utrecht, The Netherlands). The mononuclear fraction was separated using Ficoll-paque (GE17-5446, Sigma-Aldrich) and selected based on their plastic adherence. MSCs were cultured in a humidified incubator at 37 °C and 5% CO_2 with MSC expansion medium consisting of α-MEM (22561, Gibco) supplemented with 10% FBS, 0.2 mM ASAP, 100 U/mL penicillin with 100 mg/mL streptomycin and 1 ng/ml bFGF. The medium was refreshed three times per week and MSCs were passaged at subconfluency. Subsequently, MSC multilineage potential was confirmed as previously described [39]. MSCs were used for experiments at passage 4.

For the experiments, ACs and MSCs were pelleted by centrifugation at 300 g for 6 min at a density of 2×10^5 and 2.5×10^5 cells per pellet, respectively. Subsequently, AC pellets were cultured in high glucose DMEM medium containing 100 U/mL penicillin and 100 mg/mL streptomycin, 0.2 mM ASAP, 1× insulin-transferrin-selenium-ethanolamine (ITS-X, 51500056, Gibco), and 50 µg/mL L-proline (P0380, Sigma-Aldrich) in a humidified incubator at 37 °C and 5% CO_2. MSCs were cultured in chondrogenic differentiation medium, consisting of high glucose DMEM supplemented with 1% ITS premix (354352, Corning), 10^{-7} M dexamethasone (D8893, Sigma), 100 U/mL penicillin and 100 mg/mL streptomycin, and

0.2 mM ASAP. Pellets of ACs and MSCs were cultured for 14, 21 and 28 days in the presence or absence of 10 ng/ml of transforming growth factor beta 1 (TGF-β1, 240-B, R&D Systems).

2.2. Cytotoxicity

The contrast agent CA4+ (MW = 1354 g/mol, q = +4) was synthesized and provided by the lab of Mark W. Grinstaff [30]. Cytotoxicity of CA4+ was examined by measuring the activity of lactate dehydrogenase (LDH) and assessing metabolic activity of the cells by the Alamar Blue assay. At day 0, 12,000 primary human OA chondrocytes were plated in ultra-low attachment 96-well plates and incubated for 24 h in DMEM medium containing 100 U/mL penicillin and 100 mg/mL streptomycin, 0.2 mM ASAP, 1x ITS-X, and 50 µg/mL L-proline. Subsequently, CA4+ was added to the cells at different concentrations of 2, 4, 8, 16 and 20 and 30 mg iodine per ml (mgI/ml) followed by 3 or 24 h incubation. Cells non-exposed to CA4+ were used as negative control. Upon incubation, conditioned medium was collected and analysed for LDH activity using the Cytotoxicity Detection KitPLUS (4744926001, Roche) following the manufacturer's instructions. Cytotoxicity was expressed as a percentage of the (maximum) toxicity in cells treated with 0.15% Triton X-100, according to the manufacturer's instructions.

The medium was then changed to culture medium containing 10% (v/v) Alamar Blue and incubated overnight. Fluorescence of the medium (ex = 544 nm, em = 620 nm) was measured in a microplate reader (Fluoroskan Ascent, ThermoFisher Scientific). The metabolic activity was expressed as a percentage of the viability of untreated cells. Experiments were repeated for three different donors. CA4+ was shown not to interfere with Alamar Blue measurements (Fig. S1).

2.3. CA4+ incubation and µCT scanning

Pellets were incubated in a solution containing 4 mgI/ml CA4+ in culture medium for 3 h. After incubation, the medium was removed from the culture tube and µCT was performed at voxel size of 20 μm^3 in four different protocols, namely I) 90 kV tube voltage with i) 3 min and ii) 26 s scan time, and II) 70 kV tube voltage with i) 3 min and ii) 26 s scan time, all under 200 µA tube current. The mentioned tube voltages were chosen to achieve a higher signal-to-noise ratio, and hence better resolution and sensitivity. The samples were scanned in 15 ml falcon tubes and, before imaging, medium was removed, however complete removal of the CA4+ solution was not observed. Scanning was performed using a micro-computed tomography scanner (µCT, Quantum FX, Perkin Elmer, USA). 3D reconstruction was carried out automatically after completion of each scan using the scanner's software (Quantum FX µCT software, Perkin Elmer, USA). A phantom series of CA4+ at increasing concentrations (0, 2.5, 5, 10, 20 and 40 mgI/ml) was used to normalize the grey values measured within the pellets, and hence convert them to CA4+ concentrations. To this end, three regions of interest were taken for each pellet and average pixel value was converted to average CA4+ concentration, based on the phantom series. CA4+ content was calculated by multiplying average CA4+ concentration in the pellets by pellet volume (Eq. (1)) obtained by global segmentation upon applying a noise removal filter using Fiji (software version 1.50, National Institutes of Health, Bethesda, USA) and BoneJ plugin [40,41].

$$CA4^{+}\ content\ =\ CA4^{+}\ concentration\ \times\ Pellet\ volume \quad (1)$$

After scanning, 300 µl of plain medium was added to the pellets overnight to promote washing out of the CA4+, thus preventing interference with DMMB. Upon washing, pellets were digested with papain and GAGs were measured using DMMB. DMMB was additionally performed on the washing media. Total GAGs were then plotted against CA4+ content. Experiment was performed in triplicate and samples were pooled for linear regression analysis. The equation obtained from the CA4+/GAG linear regression was used to obtain predicted GAG content values in subsequent experiments. For validation of the established equation, a different set of pellets was scanned upon culturing. After scanning, pellets were digested in papain followed by DMMB assay. The measured GAG values were plotted against predicted values obtained using the established equation.

X-ray doses of each scanning protocol were measured using RaySafe Solo (Ray Safe, Sweden) dosimeter.

2.4. Dynamic and longitudinal assessment of GAG content and distribution

Human ACs were pelleted and cultured as described in Section 2.3. Pellets were cultured for a total of 31 days. Culture medium was collected and replaced twice a week. CA4+ incubation and µCT scanning were performed at days 14, 21 and 28. A day before scanning, medium was replaced by medium containing 10% (v/v) Alamar Blue followed by overnight incubation. The day after, metabolic activity was evaluated by measuring fluorescence in the medium as mentioned in Section 2.2. The pellets were then incubated with 300 µl of 4 mgI/ml CA4+ for 3 h and subsequently scanned at 70 kV tube voltage for 26 s. After scanning, pellets were washed twice in 600 µl of plain medium for 1 and 3 h, respectively. The washing was performed to ensure faster and more efficient removal of CA4+ to decrease the probability of cytotoxic effects and interference with subsequent µCT scans. Metabolic activity was again measured post-scanning. DMMB was performed in the collected medium every 3 or 4 days to quantify GAG release. At the end of the 32-day culture period, pellets were digested and processed for GAG and DNA analysis by DMMB and PicoGreen, respectively. Non-treated (no scan and no CA4+) pellets as well as pellets exposed to scanning or CA4+ incubation alone were taken as controls to evaluate their individual effects on metabolic activity. A longitudinal scheme of the experiment is depicted in Fig. 4a.

2.5. Comparison between histology and µCT imaging

Human ACs and MSCs were pelleted and cultured for 14 days as described above in the absence or presence of TGF-β. Additionally, as a more relevant tissue culture model, MSCs were cultured in collagen type I hydrogels. To fabricate the hydrogels, $1*10^6$ MSCs (cell density of $20*10^6$ cells/ml) were mixed with 50 μl of a 4 mg/ml collagen type I solution (Corning, 354249), which was allowed to gel for one hour at 37 °C, 5% CO_2. Upon gelation, hydrogels were cultured in chondrogenic medium in the presence of 10 ng/ml TGF-β for 28 days.

At the endpoint, the constructs were incubated with 4 mgI/ml CA4+ for 3 h. After incubation, the medium was removed and pellets were embedded in TissueTek (4593, Sakura) and snap frozen in cryomolds (10 mm × 10 mm × 5 mm) using liquid nitrogen. The slab shape of the mold guaranteed that the constructs were scanned and sectioned in the same orientation and direction. Constructs were frozen in pairs to facilitate adjustments regarding the orientation after sectioning (by using one pellet as reference for relative position) as depicted in Fig. S2. µCT was performed at voxel size of 20 μm^3 at a 70 kV tube voltage for both 26 s and 3 min under 200 µA tube current. During scanning samples were kept frozen using dry ice.

After scanning, pellets were sectioned using a cryotome. Four sections of 10 µm were collected every 100 µm. Sectioning was performed according to the coordinates of the µCT slices.

Safranin-O/Fast-Green staining was performed to stain GAGs in the pellet sections with Mayer's hematoxylin counterstaining of

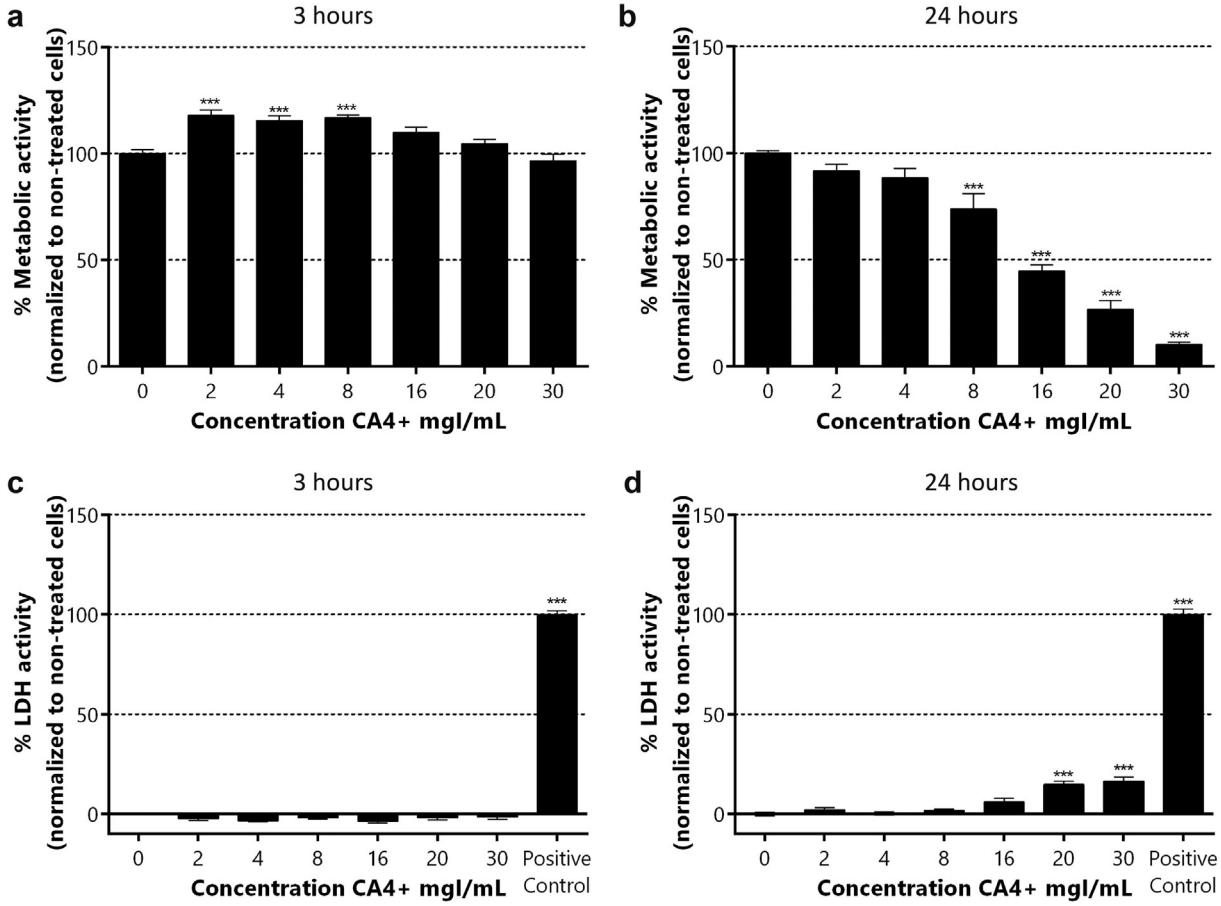

Fig. 1. Effect of CA4+ on the viability of human chondrocytes. Metabolic activity and LDH activity measured after 3 (a and c) and 24 (b and d) hours incubation with CA4+ concentrations of 2, 4, 8, 16, 20 and 30 mgI/mL. Cells without CA4+ were used as controls. A solution of 0.15% Triton-X was used as positive control for complete cell lysis. Data are represented as mean ± standard deviation (SD). Experiment was performed in three biological replicates ($n = 3$). * represents statistically significant differences compared to non-treated cells (0 mgI/ml CA4+). ($^{*}p < 0.05$, $^{**}p < 0.01$ and $^{***}p < 0.001$).

nuclei. The sections were imaged with a light microscope (BX51, Olympus, The Netherlands). Images were acquired with a 1.25x magnification. Histological images were first aligned and then compared to their corresponding slices in the µCT stacks using Fiji.

2.6. Statistical analysis

All data were analysed using IBM® SPSS® Statistics version 21. Cytotoxicity on monolayer was analysed by univariate analysis of variance using a randomized block design. A post-hoc test with Bonferroni correction was applied for multiple comparisons between treatments (p value < 0.05).

Linear regression analysis was applied to evaluate whether the CA4+ content correlated with GAG content. The coefficient of determination (R^2) was used to assess the correlations. Significance level was set at p value < 0.05. The intra-class correlation coefficient (ICC) was used to calculate measurement reliability for the GAG prediction model. A two-way mixed-effect model based on mean-rating ($k = 2$) and absolute agreement was used, as previously described [42]. ICC estimate and the 95% confidence intervals (CI) were reported.

Data on longitudinal measurements of metabolic activity and GAG release were analysed using a linear mixed model, followed by pairwise comparison with Bonferroni adjustment (p value < 0.05). Model selection was based on the lowest Akaike Information Criterion. Donor served as random effect factor and condition, days and their interaction served as fixed effect factors. Regression coefficients were estimated by the maximum likelihood method.

Accuracy of the established equation was evaluated by Pearson's correlation. Additionally, relative error was calculated for each measurement, according to the following formula (Eq. (2)):

$$Relative\ error = \frac{|Predicted\ value - Real\ value|}{Real\ value} \times 100 \quad (2)$$

Differences in total GAG content and GAG/DNA ratio between the treatment conditions were determined by univariate analysis of variance using a randomized block design. The data were first logarithmically transformed so the assumptions of normality of residuals and homogeneity of variances were met. A post-hoc test with Bonferroni correction was applied for multiple comparisons (p value < 0.05),

3. Results

3.1. Cytotoxicity

To determine the boundary concentration of CA4+ in terms of cytotoxicity, ACs were incubated with increasing concentrations of CA4+ (2–30 mgI/mL) for 3 and 24 h.

With concentrations up to 30 mgI/mL and 3 h incubation, no cytotoxic effects were detected at metabolic activity and LDH activity levels, yet an increased metabolic activity was observed for concentrations up to 8 mgI/ml (Fig. 1a and 1c). However, longer incubation times (24 h) led to a decrease in metabolic activity at

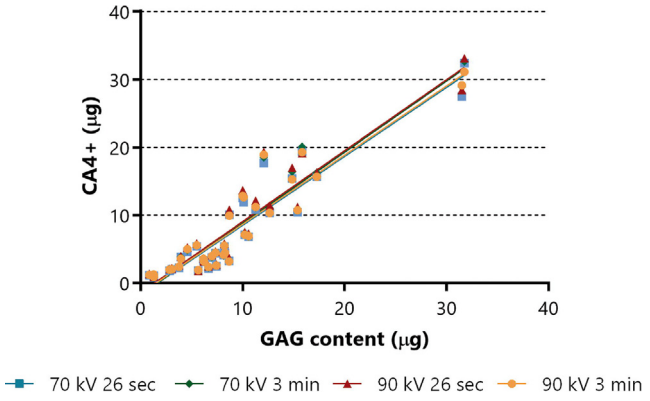

Fig. 2. Correlation between CA4+ and total GAG contents upon 3 h incubation. CA4+ and GAG contents of pellets were determined by μCT and DMMB, respectively. CA4+ content values were plotted against total GAG content for each scanning protocol and data was fitted by linear regression. Colored lines represent linear regression for each scanning protocol. Data presented here were pooled from three independent experiments.

Table 1
Linear regression of CA4+ concentration with total GAG content.

Scanning Protocol (X-ray dose, mGy)	Equation	R^2	p value
70 kV 26 s (29.50 mGy)	$GAGs = \frac{CA4^+ + 1.67}{1.01}$ (3)	0.88	<0.0001
70 kV 3 min (184.90 mGy)	$GAGs = \frac{CA4^+ + 1.70}{1.05}$ (4)	0.88	<0.0001
90 kV 26 s (47.65 mGy)	$GAGs = \frac{CA4^+ + 1.42}{1.05}$ (5)	0.87	<0.0001
90 kV 3 min (431.50 mGy)	$GAGs = \frac{CA4^+ + 1.54}{1.02}$ (6)	0.87	<0.0001

concentrations above 8 mgI/mL (Fig. 1b). Furthermore, LDH activity increased above a CA4+ concentration of 20 mgI/mL (Fig. 1d).

3.2. Correlation between CA4+ and GAG contents

AC pellets cultured in presence or absence of 10 ng/mL TGF-β for 14, 21 and 28 days were used to evaluate the relationship between CA4+ and GAG content. The CA4+ content within the pellets linearly related with the total GAG content as measured by DMMB (Fig. 2). Linear regression analysis showed R^2 values above 0.87 and p values < 0.0001 for all the scanning protocols (Table 1). The scanning protocol with a tube voltage of 70 kV and a scanning time of 26 s was as effective as the other protocols, and was shown to yield a lower X-ray dose (Table 1).

Additionally, pellet volume increased with GAG content (Fig. S3). Importantly, CA4+ incubation yielded a maximum concentration of 15 mgI/mL CA4+ within the pellets (Fig. S4), which was shown to be cytocompatible. In subsequent experiments, 4 mgI/mL CA4+ concentration and a scanning protocol of 70 kV 26 s were used, the latter to minimize radiation dose.

To validate the accuracy of the model, a different set of pellets was scanned after 3 h of incubation with 4 mgI/mL CA4+ and subsequently washed, digested and analyzed with DMMB. Predicted GAG content was calculated using Eq. (3) from Table 1, and plotted against real GAG content as measured by DMMB (Fig. 3a). A significant correlation was observed (Pearson $r = 0.92$, $p = 0.0001$), and the mean relative error was shown to be 22% (Fig. 3b). The relative error became negative with higher GAG contents, indicating an underestimation for these samples. The ICC value for inter-measurement reliability was 0.884, indicating a good agreement between the two predicted and measured GAGs.

3.3. Longitudinal monitoring of chondrogenic pellets

To evaluate whether this method could be used for real-time and longitudinal measurements of GAG production, pellets were cultured for 31 days, and scanned at 14, 21 and 28 days.

The metabolic activity of the pellets was shown to be unaffected by both the μCT scanning and the CA4+ incubation, when compared to control pellets (Fig. 4b). A statistically significant higher metabolic activity is observed between the pellets exposed only to the scanning procedure and the remaining conditions at days 21, 28 and 29 ($p < 0.05$).

GAG release into the media was shown to be unaffected by CA4+ incubation plus scanning when compared to control pellets, further suggesting the protocol does not affect GAG production (Fig. 4c). A significantly higher GAG release was observed for pellets only exposed to scanning in comparison with the remaining conditions from day 17 onwards. Despite these effects during culture, at the end of the culture period, neither GAG nor GAG/DNA levels were significantly different across the different conditions (Fig. 4d and 4e). Similarly, DNA levels were also not affected by CA4+ and/or scanning (Fig. S5). The washing protocol was shown to be effective for CA4+ removal, with most of the contrast agent being washed out of the pellets after 3 h, and with X-ray

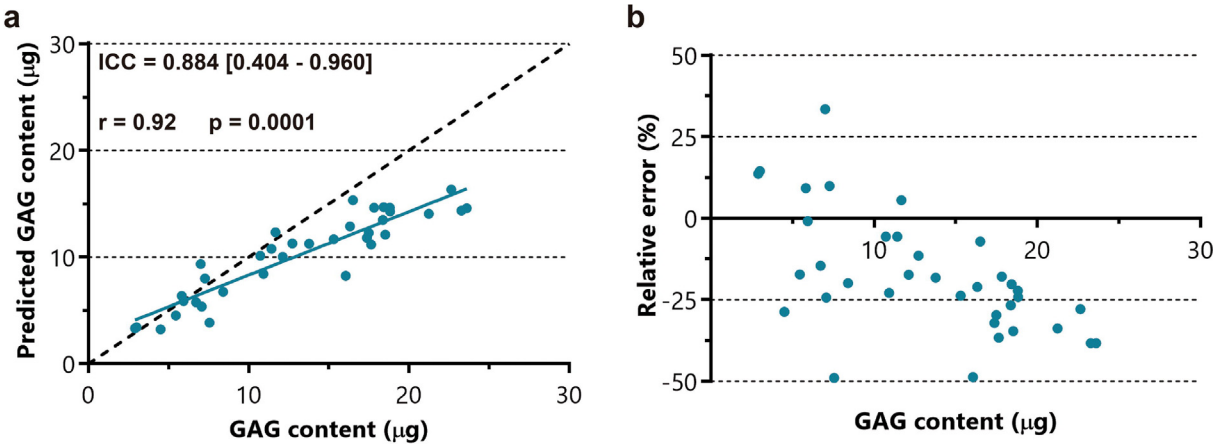

Fig. 3. Validation of the prediction model. Pellets were scanned using 70 kV tube voltage and 26 sec acquisition time upon 3 h incubation with 4 mgI/mL CA4+. a) DMMB-determined GAG values were plotted against predicted values using Eq. (3) from Table 1. Dashed line represents theoretical complete match between predicted and real values ($y = x$). b) Relative error calculated based on real GAG content.

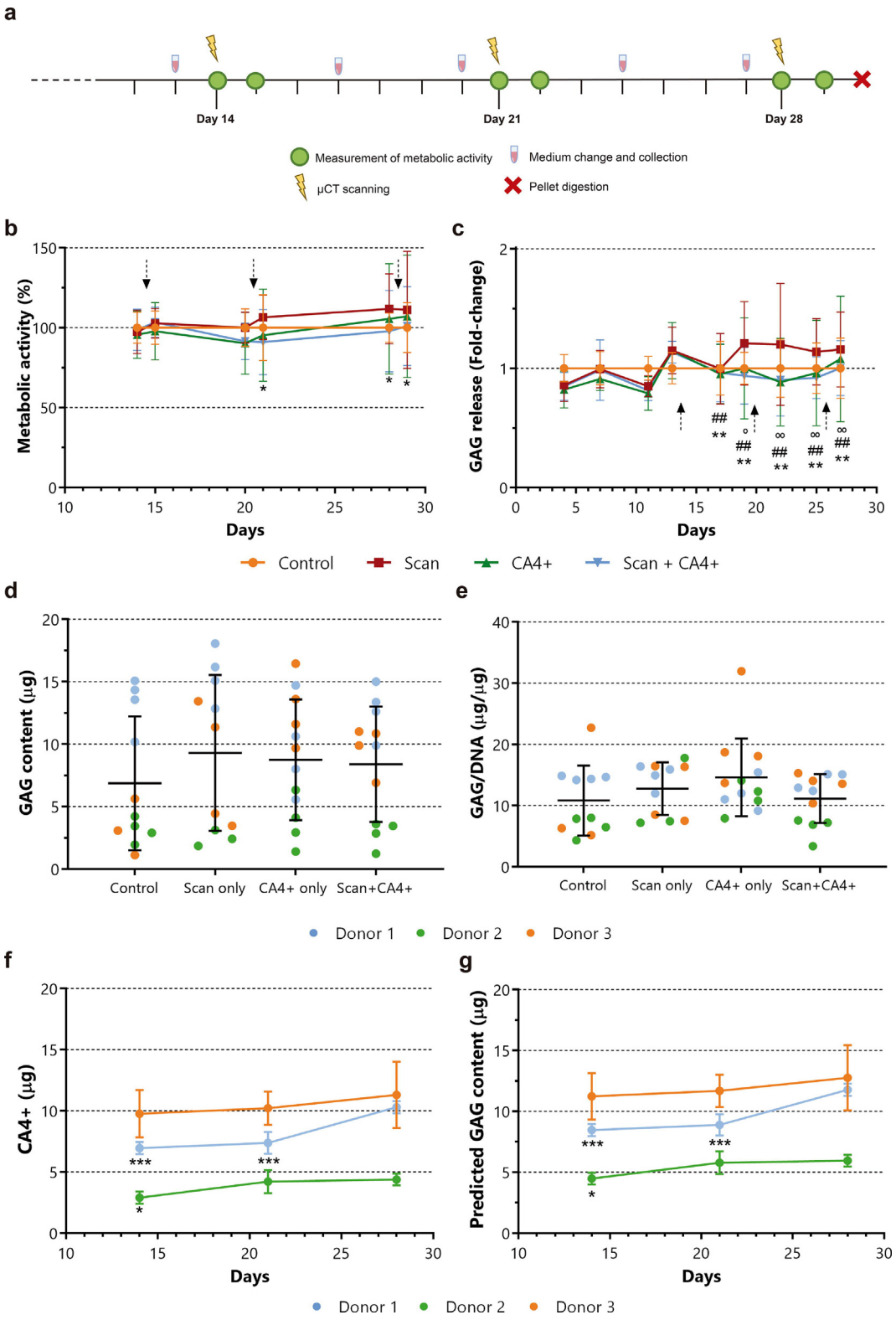

Fig. 4. CECT-based longitudinal determination of total GAG content in chondrogenic pellets. a) Schematic representation of longitudinal monitoring of chondrogenic pellets. b) Metabolic activity of chondrogenic pellets measured before and after µCT scanning and CA4+ incubation. Data are represented as percentage of metabolic activity of control pellets ($n = 3$). c) GAG release. Data are represented as fold-change compared to the untreated control pellets at the same time point ($n = 3$). Arrows represent timing of CA4+ incubation and/or scanning. * represents statistically significant differences between the "Scan" and "Scan + CA4+" pellets. # represents statistically significant difference between the "Scan" and "CA4+" pellets. ° represents statistically significant difference between the "Scan" and "Control" groups. ($^{*}p < 0.05$, $^{**}p < 0.01$ and $^{***}p < 0.001$). d) Total GAG content measured by DMMB after a 30-day culture period. e) GAG/DNA content measured after a 30-day culture period. Data are presented by mean ± SD. Note that colour legends differ between figures b, c and d, e, f and g. f) CA4+ content within pellets determined using tube voltage of 70 kV and acquisition time of 26 s. g) Predicted total GAG content calculated based on Eq. (3), describing the CA4+ vs. GAG correlation determined using tube voltage 70 kV and 26 s acquisition time. * represents statistically significant differences between days 14 or 21 and day 28. ($^{*}p < 0.05$ and $^{***}p < 0.001$).

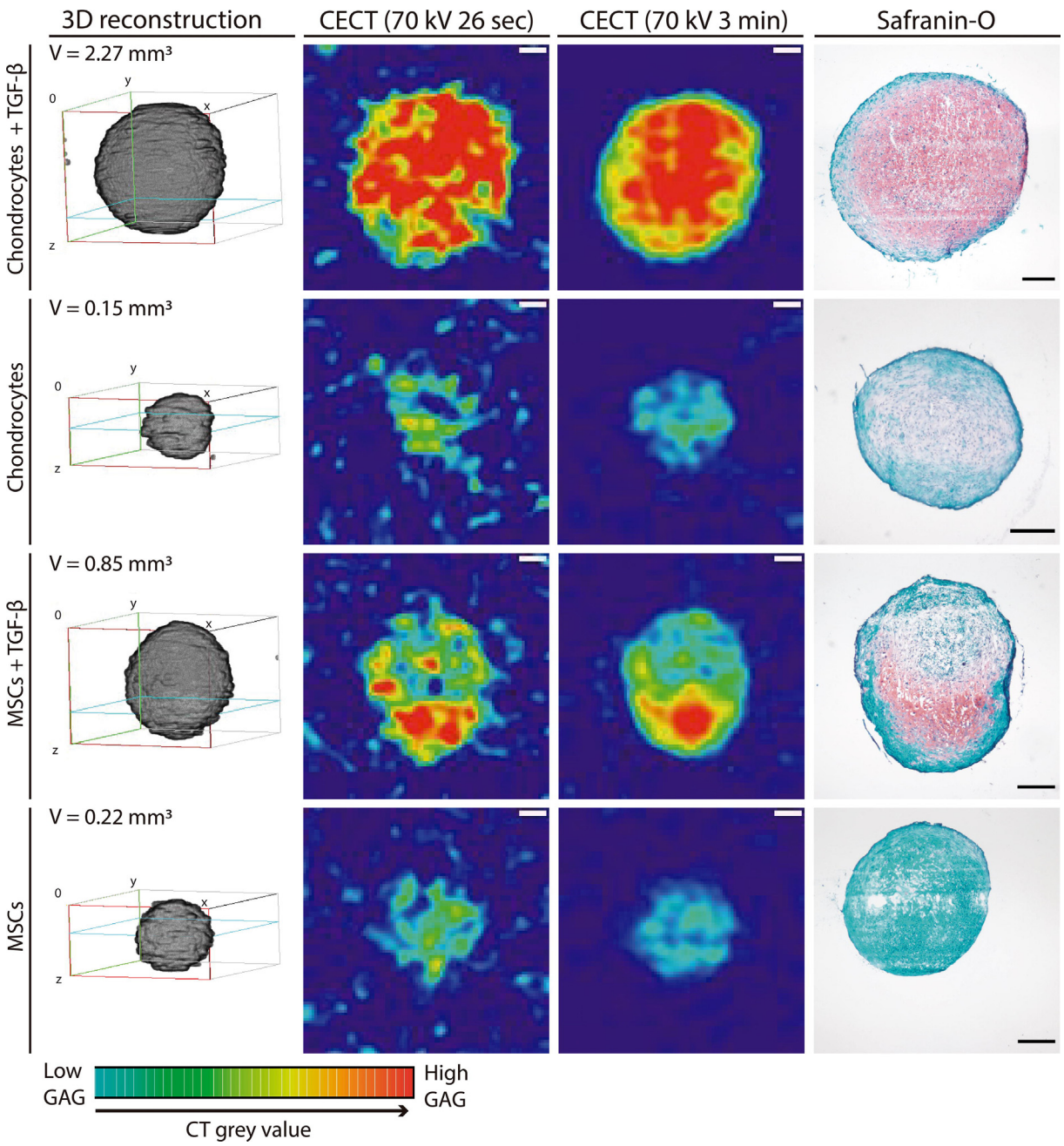

Fig. 5. Comparison between CA4+ and GAG distributions. Pellets were scanned at 70 kV for i) 26 s and ii) 3 min upon 3 h incubation with 4 mgI/mL CA4+. Scale bar: 200 µm.

absorption values returning to baseline after an overnight washing step (Fig. S6).

Finally, the X-ray absorption values were converted into CA4+ content (Fig. 4f) by multiplying the CA4+ concentration by the pellet volume. Subsequently, CA4+ content was used to predict total GAG content (Fig. 4g) using the previously established equation (Eq. (3)):

$$GAGs = \frac{CA4^{+} + 1.67}{1.01} \quad (3)$$

As shown in Fig. 4f and 4g, there was a trend for increasing CA4+ content throughout the culture period, reflecting an increase in GAG content.

3.4. CA4+ spatial distribution vs. safranin-O histology

As seen in Fig. 5, CA4+ distribution via CECT matched with GAG distribution as determined by safranin-O staining. While chondrocyte pellets showed a more homogeneous GAG distribution, MSCs yielded pellets with more heterogenous GAG distribution. On the other hand, chondrocytes and MSCs that were not chondrogenically differentiated showed a very low CA4+ signal that matched the absence of safranin-O staining. The distribution of CA4+ matched safranin-O histology independently of scanning time, yet with a lower signal to noise ratio for the protocol using 26 s acquisition time (Fig. 5). Furthermore, CECT allowed for 3D reconstruction of the construct, providing information on 3D GAG

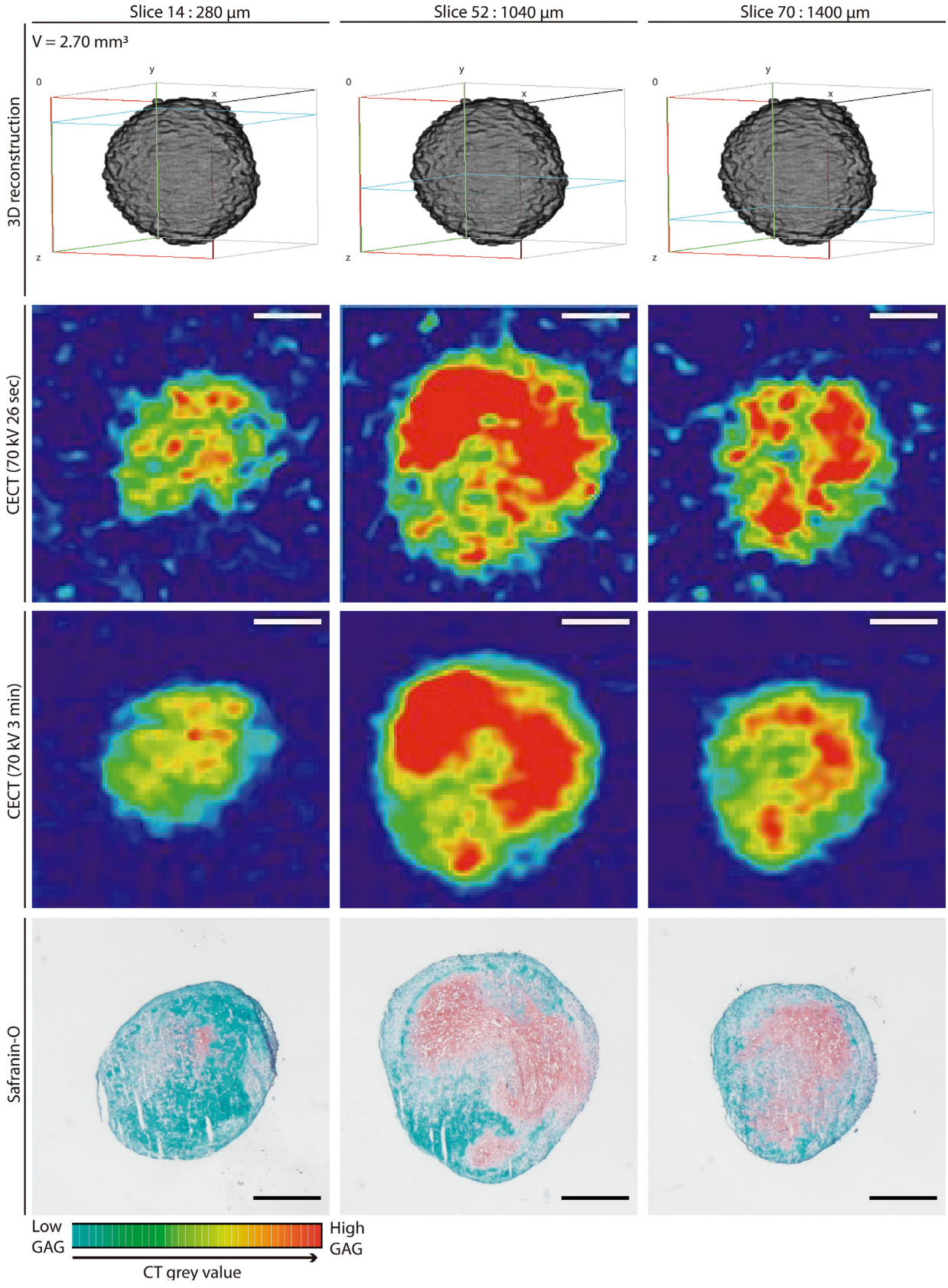

Fig. 6. 3D reconstruction of CA4+ and GAG distribution in a collagen gel containing MSCs. Gels were scanned at 70 kV for i) 26 s and ii) 3 min upon 3 h incubation with 4 mgI/mL CA4+. Slice number indicates the distance from the upper part of the construct. Blue line (top row) identifies the slice corresponding to the CECT and safranin-O images. Scale bar: 500 µm. (For interpretation of the references to colour in this figure legend, the reader is referred to the web version of this article.)

distribution and construct volume. Also, tests on collagen hydrogels containing chondrogenically differentiated MSCs showed that CA4+ distribution matched the safranin-O staining pattern (Fig. 6, Supplementary Movie 1).

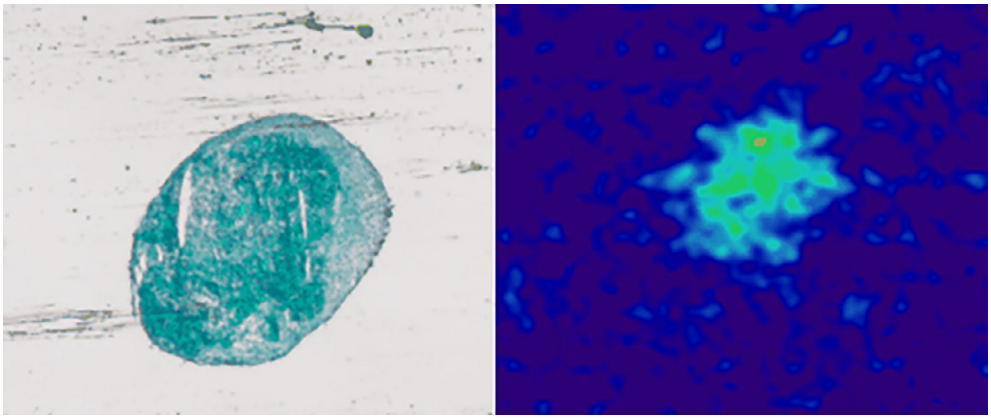

Supplementary Movie 1.

4. Discussion

Musculoskeletal diseases such as OA or cartilage injuries are in need of new therapies, and tissue engineering and regenerative medicine strategies hold significant promise [5]. However, for these strategies to rapidly progress to the clinic, additional quantitative techniques and tools are needed for the 3D and longitudinal monitoring of *in vitro* regeneration [33,8,43]. To this end, we show proof-of-concept for the applicability of a CECT-based method, by demonstrating a correlation between CA4+ concentration and total GAG content, and its subsequent use to predict total GAG content at different timepoints. As mentioned previously, it is crucial for such method to be non-destructive and compatible with cell culture. Hence, we firstly looked at the effect of CA4+ exposure on cell viability. Concentrations above 8 mgI/mL and an exposure of 24 h led to significant negative effects on cell viability, which was likely caused by the cationic nature of the CA4+. In fact, cationic molecules and particles are known to promote cellular toxicity through interaction with and disruption of the cellular membrane [44]. Shortening the incubation time and lowering the concentration of CA4+ decreased the risk of over-exposure and hence reduced cytotoxicity. While *in vitro* toxicity of CA4+ has not been reported, previous studies on cartilage explants used incubation periods of up to 24 h and CA4+ concentrations of 12 and 27 mgI/mL [35,36,38]. In two studies on mouse cartilage (100 µm thickness), a period of 40 min was used to ensure sufficient diffusion of CA4+ at a bath concentration of 12 mgI/ml [37,45]. Similar results were found for rabbit articular cartilage (400–500 µm) where a period of 40 min was sufficient for CA4+ to reach a plateau concentration within the cartilage [46]. For the pellet constructs in this study, an incubation time of 3 h with CA4+ at 4 mgI/mL was selected. While it is true that diffusion will still occur after 3 h, a strong and linear correlation was observed between CA4+ and total GAG content with this incubation time. Additionally, bearing in mind that CA4+ was shown to be cytotoxic after 3 h incubation, we believe longer incubation times could lead to matrix degradation, hence compromising the CA4+/GAG relationship.

For subsequent experiments, the scanning protocol with a tube voltage of 70 kV and 26 s, plus a CA4+ concentration of 4 mgI/mL and 3 h incubation were chosen. Validation of the technique with the previously described parameters and a different set of samples corroborated its suitability for the determination of total GAG content based on a CA4+ concentration of 4 mgI/mL and 3 h incubation. The ICC between predicted and measured GAG content was shown to be 0.884, indicating a good agreement and reliability between measurements [42]. However, the proposed technique is not free of error as we observed an average error for predicted GAG content of 22%. Likely, part of the error arises from discrepancies associated with pellet volume measurements using µCT data with suboptimal spatial resolution. Hence, enhanced spatial resolution may improve pellet segmentation, which can help minimizing volume measurement error. Additionally, the differences in total GAG content distribution observed between the regression model and its validation can partially explain the obtained error. However, the increasing values of CA4+ content with developing chondrogenic pellets corroborates the robustness of the technique to predict GAG content longitudinally. For future studies, a higher number of constructs containing a wider range of GAG content should be used to reduce errors between regression and prediction experiments.

Subsequently, the feasibility of using such model for real-time measurements of GAG production in chondrogenic pellets was assessed. Optimization of scanning parameters and incubation protocols rendered the protocol non-toxic and harmless to chondrogenesis, as measured by GAG production. The proposed protocol was found to be cytocompatible, with no deleterious effects on the metabolic activity of chondrogenic pellets after multiple exposures to X-rays and CA4+ (70 kV, 26 s/4 mgI/mL CA4+, 3 h). Most importantly, no significant changes were found at the endpoint on the total GAG and GAG/DNA content across conditions, proving that this method is compatible with chondrogenic culture and differentiation.

Additionally, the proposed technique allowed for quantitative and 3D imaging, not only in pellets but also in more complex and relevant tissue culture models such as hydrogels, offering insight on the 3D distribution and organization of GAGs. Comparison between CECT images and safranin-O staining on tissue sections showed that CA4+ distribution closely reflects GAG localization and distribution within the constructs, allowing for “3D histological” evaluation. Noteworthy, the proposed technique offers the unparalleled features of not only being non-destructive but also being time-efficient compared to conventional safranin-O histology which carries the risk of sectioning artifacts while being destructive and labor-intensive [9,18,43].

The scanning protocol yielded X-ray doses of approximately 30 mGy, which is lower than those reported to be cytotoxic and

anti-chondrogenic for chondrocytes [47–51]. A single dose of 2 or 10 Gy was reported to cause no deleterious effects on GAG synthesis or deposition in chondrocytes cultured in pellets [50]. On the contrary, proliferation and DNA synthesis were halted temporarily and permanently with 2 and 10 Gy doses, respectively [50]. In another study, even though MSC viability was shown to remain unaffected by a 2 Gy dose, there was a decreased expression of chondrogenic markers such as aggrecan and type II collagen [51]. Importantly, most studies often report X-ray doses of 1 Gy and above, which are at least 30 times higher than the dose used in this study. Accordingly, we did not see any negative effects of μCT imaging on cell viability or DNA content. However, we did observe an increased GAG release for scanned pellets without CA4+. Although final GAG content was not altered, it is still to be clarified whether lower X-ray doses can stimulate GAG production. Moreover, additional studies are needed to gain insight on the long-term effects of low X-ray and CA4+ exposures on cells within tissues. Such studies should address DNA damage or mutations, as well as the effects on chondrogenic markers and differentiation.

For the implementation of the proposed technique a few considerations should be considered. Firstly, validation and/or optimization of the method should be performed for every construct type, as diffusion is dependent on construct size and matrix composition [52–54]. As shown before, diffusion time increases relatively to the square of the tissue thickness [55,56]. Another important step in the protocol is the washout of CA4+, as accumulation within the construct may lead to toxicity and ultimately affect chondrogenesis, and preclude accurate real-time measurement of CA4+ and hence GAG content. Additionally, retention of the CA4+ within the construct might affect subsequent scans. A single solution of contrast agent should be prepared at the start of the experiment to avoid discrepancies in dilutions and between sequential measurements, which can potentially lead to differences in grey values and therefore negatively affect the GAG vs CA4+ correlation. Finally, automatization of image processing and analysis will additionally render the protocol more sensitive and accurate.

Given our successful study with chondrocytes and MSCs based pellets, this method for monitoring GAG production is likely advantageous for other cartilage tissue-engineered constructs based on biomaterials such as hydrogels and bioprinted scaffolds. Additionally, future studies should examine its utility in other tissue-engineered tissues such as the cornea [57,58], intervertebral discs [59,60], and heart valves [61,62], where GAGs are known to play crucial morphological and physiological roles. The proposed method is also of potential use as a pre-implantation tool, where constructs are screened prior to implantation in an animal model. When implemented, this method may offer unprecedented insight on chondrogenic development within cartilage-engineered constructs and facilitate the advancement of such therapies to the clinic. In conclusion, CA4+-based CECT is a useful and non-destructive quantitative technique for 3D imaging and longitudinal assessment of GAG production and distribution in cartilage tissue engineering.

Declaration of Competing Interest

The authors declare that they have no known competing financial interests or personal relationships that could have appeared to influence the work reported in this paper.

Acknowledgments

This project has received funding from the European Union's Horizon 2020 research and innovation programme under Marie Sklodowska-Curie grant agreement No. 642414 and the Dutch Arthritis Foundation (LLP12). We thank Dr. Amit Patwa for synthesizing the CA4+. We thank Dr. Casper Beijst for the help with X-ray dose measurements. We thank Luís Garcia for providing the illustration for the graphical abstract.

Data availability

We confirm that all relevant data are available from the authors.

Appendix A. Supplementary data

Supplementary data to this article can be found online at https://doi.org/10.1016/j.actbio.2019.09.014.

References

[1] A.D. Woolf, B. Pfleger, Burden of major musculoskeletal conditions, Bull. World Health Org. 81 (2003) 646–656.
[2] M.B. Goldring, S.R. Goldring, Osteoarthritis, J. Cell. Physiol. 213 (2007) 626–634.
[3] J. Lieberthal, N. Sambamurthy, C.R. Scanzello, Inflammation in joint injury and post-traumatic osteoarthritis, Osteoarthritis Cartilage 23 (2015) 1825–1834.
[4] M.B. Goldring, F. Berenbaum, Emerging targets in osteoarthritis therapy, Curr. Opin. Pharmacol. 22 (2015) 51–63.
[5] C. Chung, J.A. Burdick, Engineering cartilage tissue, Adv. Drug Del. Rev. 60 (2008) 243–262.
[6] R.W. Farndale, D.J. Buttle, A.J. Barrett, Improved quantitation and discrimination of sulphated glycosaminoglycans by use of dimethylmethylene blue, Biochim. Biophys. Acta 883 (1986) 173–177.
[7] G.K. Reddy, C.S. Enwemeka, A simplified method for the analysis of hydroxyproline in biological tissues, Clinical Biochemistry 29 (1996) 225–229.
[8] A.A. Appel, M.A. Anastasio, J.C. Larson, E.M. Brey, Imaging challenges in biomaterials and tissue engineering, Biomaterials 34 (2013) 6615–6630.
[9] G. Kerckhofs, S. Stegen, N. van Gastel, A. Sap, G. Falgayrac, G. Penel, M. Durand, F.P. Luyten, L. Geris, K. Vandamme, T. Parac-Vogt, G. Carmeliet, Simultaneous three-dimensional visualization of mineralized and soft skeletal tissues by a novel microCT contrast agent with polyoxometalate structure, Biomaterials 159 (2018) 1–12.
[10] B.Z. Fite, M. Decaris, Y. Sun, Y. Sun, A. Lam, C.K. Ho, J.K. Leach, L. Marcu, Noninvasive multimodal evaluation of bioengineered cartilage constructs combining time-resolved fluorescence and ultrasound imaging, Tissue Eng. Part C Methods 17 (2011) 495–504.
[11] S. Kreitz, G. Dohmen, S. Hasken, T. Schmitz-Rode, P. Mela, S. Jockenhoevel, Nondestructive method to evaluate the collagen content of fibrin-based tissue engineered structures via ultrasound, Tissue Eng. Part C Methods 17 (2011) 1021–1026.
[12] Y. Sun, D. Responte, H.T. Xie, J. Liu, H. Fatakdawala, J. Hu, K.A. Athanasiou, L. Marcu, Nondestructive evaluation of tissue engineered articular cartilage using time-resolved fluorescence spectroscopy and ultrasound backscatter microscopy, Tissue Eng. Part C Methods 18 (2012) 215–226.
[13] C.X. Deng, X. Hong, J.P. Stegemann, Ultrasound Imaging Techniques for Spatiotemporal Characterization of Composition, Microstructure, and Mechanical Properties in Tissue Engineering, Tissue Eng. Part B Rev. 22 (2016) 311–321.
[14] M.A. Rice, K.R. Waters, K.S. Anseth, Ultrasound monitoring of cartilaginous matrix evolution in degradable PEG hydrogels, Acta Biomater. 5 (2009) 152–161.
[15] D. Correa, R.A. Somoza, A.I. Caplan, Nondestructive/noninvasive imaging evaluation of cellular differentiation progression during in vitro mesenchymal stem cell-derived chondrogenesis, Tissue Eng. Part A 24 (2018) 662–671.
[16] L.K. Narayanan, T.L. Thompson, R.A. Shirwaiker, B. Starly, Label free process monitoring of 3D bioprinted engineered constructs via dielectric impedance spectroscopy, Biofabrication 10 (2018) 035012.
[17] H. Lusic, M.W. Grinstaff, X-ray-computed tomography contrast agents, Chem. Rev. 113 (2013) 1641–1666.
[18] A.W. Palmer, R.E. Guldberg, M.E. Levenston, Analysis of cartilage matrix fixed charge density and three-dimensional morphology via contrast-enhanced microcomputed tomography, Proc. Natl. Acad. Sci. U.S.A. 103 (2006) 19255–19260.
[19] H.T. Kokkonen, A.S. Aula, H. Kroger, J.S. Suomalainen, E. Lammentausta, E. Mervaala, J.S. Jurvelin, J. Toyras, Delayed computed tomography arthrography of human knee cartilage in vivo, Cartilage 3 (2012) 334–341.
[20] R.C. Stewart, P.N. Bansal, V. Entezari, H. Lusic, R.M. Nazarian, B.D. Snyder, M.W. Grinstaff, Contrast-enhanced CT with a high-affinity cationic contrast agent for imaging ex vivo bovine, intact ex vivo rabbit, and in vivo rabbit cartilage, Radiology 266 (2013) 141–150.
[21] T. Maerz, M.D. Newton, H.W. Matthew, K.C. Baker, Surface roughness and thickness analysis of contrast-enhanced articular cartilage using mesh parameterization, Osteoarthritis Cartilage 24 (2016) 290–298.
[22] B.A. Lakin, B.D. Snyder, M.W. Grinstaff, Assessing cartilage biomechanical properties: techniques for evaluating the functional performance of cartilage in health and disease, Annu. Rev. Biomed. Eng. 19 (2017) 27–55.
[23] B.A. Lakin, D.J. Grasso, R.C. Stewart, J.D. Freedman, B.D. Snyder, M.W. Grinstaff, Contrast enhanced CT attenuation correlates with the GAG content of bovine meniscus, J. Orth. Res. 31 (2013) 1765–1771.

[24] J.T.J. Honkanen, M.J. Turunen, J.D. Freedman, S. Saarakkala, M.W. Grinstaff, J.H. Ylarinne, J.S. Jurvelin, J. Toyras, Cationic contrast agent diffusion differs between cartilage and meniscus, Annu. Rev. Biomed. Eng. 44 (2016) 2913–2921.
[25] D.J. Oh, B.A. Lakin, R.C. Stewart, M. Wiewiorski, J.D. Freedman, M.W. Grinstaff, B.D. Snyder, Contrast-enhanced CT imaging as a non-destructive tool for ex vivo examination of the biochemical content and structure of the human meniscus, J. Orth. Res. 35 (2017) 1018–1028.
[26] T. Maerz, M.D. Newton, K. Kristof, O. Motovylyak, J.S. Fischgrund, D.K. Park, K.C. Baker, Three-dimensional characterization of in vivo intervertebral disc degeneration using EPIC-muCT, Osteoarthritis Cartilage 22 (2014) 1918–1925.
[27] K.H. Lin, S.Y. Tang, The quantitative structural and compositional analyses of degenerating intervertebral discs using magnetic resonance imaging and contrast-enhanced micro-computed tomography, Ann. Biomed. Eng. 45 (2017) 2626–2634.
[28] M.D. Newton, S.E. Hartner, S. Timmons, N.D. Delaney, M.G. Pirrone, K.C. Baker, T. Maerz, Contrast-enhanced muCT of the intervertebral disc: a comparison of anionic and cationic contrast agents for biochemical and morphological characterization, J. Orth. Res. 35 (2017) 1067–1075.
[29] Y. Wang, Y.C. Huang, A.A. Gertzman, L. Xie, A. Nizkorodov, S.L. Hyzy, K. Truncale, R.E. Guldberg, Z. Schwartz, B.D. Boyan, Endogenous regeneration of critical-size chondral defects in immunocompromised rat xiphoid cartilage using decellularized human bone matrix scaffolds, Tissue Eng. Part A 18 (2012) 2332–2342.
[30] R.C. Stewart, A.N. Patwa, H. Lusic, J.D. Freedman, M. Wathier, B.D. Snyder, A. Guermazi, M.W. Grinstaff, Synthesis and preclinical characterization of a cationic iodinated imaging contrast agent (CA4+) and its use for quantitative computed tomography of ex vivo human hip cartilage, J. Med. Chem. 60 (2017) 5543–5555.
[31] B. Pouran, V. Arbabi, A.A. Zadpoor, H. Weinans, Isolated effects of external bath osmolality, solute concentration, and electrical charge on solute transport across articular cartilage, Med. Eng. Phys. 38 (2016) 1399–1407.
[32] V. Arbabi, B. Pouran, H. Weinans, A.A. Zadpoor, Multiphasic modeling of charged solute transport across articular cartilage: application of multi-zone finite-bath model, J. Biomech. 49 (2016) 1510–1517.
[33] L.H. Jin, B.H. Choi, Y.J. Kim, H.J. Oh, B.J. Kim, X.Y. Yin, B.H. Min, Nondestructive assessment of glycosaminoglycans in engineered cartilages using hexabrix-enhanced micro-computed tomography, Tissue Eng. Regen. Med. 15 (2018) 311–319.
[34] N.S. Joshi, P.N. Bansal, R.C. Stewart, B.D. Snyder, M.W. Grinstaff, Effect of contrast agent charge on visualization of articular cartilage using computed tomography: exploiting electrostatic interactions for improved sensitivity, J. Am. Chem. Soc. 131 (2009) 13234–13235.
[35] P.N. Bansal, N.S. Joshi, V. Entezari, B.C. Malone, R.C. Stewart, B.D. Snyder, M.W. Grinstaff, Cationic contrast agents improve quantification of glycosaminoglycan (GAG) content by contrast enhanced CT imaging of cartilage, J. Orth. Res. 29 (2011) 704–709.
[36] B.A. Lakin, D.J. Grasso, S.S. Shah, R.C. Stewart, P.N. Bansal, J.D. Freedman, M.W. Grinstaff, B.D. Snyder, Cationic agent contrast-enhanced computed tomography imaging of cartilage correlates with the compressive modulus and coefficient of friction, Osteoarthritis Cartilage 21 (2013) 60–68.
[37] B.A. Lakin, H. Patel, C. Holland, J.D. Freedman, J.S. Shelofsky, B.D. Snyder, K.S. Stok, M.W. Grinstaff, Contrast-enhanced CT using a cationic contrast agent enables non-destructive assessment of the biochemical and biomechanical properties of mouse tibial plateau cartilage, J. Orth. Res. 34 (2016) 1130–1138.
[38] S.S. Karhula, M.A. Finnilä, J.D. Freedman, S. Kauppinen, M. Valkealahti, P. Lehenkari, K.P.H. Pritzker, H.J. Nieminen, B.D. Snyder, M.W. Grinstaff, S. Saarakkala, Micro-scale distribution of CA4+ in ex vivo human articular cartilage detected with contrast-enhanced micro-computed tomography imaging, Front. Physics 5 (2017) 1–8.
[39] M.F. Pittenger, A.M. Mackay, S.C. Beck, R.K. Jaiswal, R. Douglas, J.D. Mosca, M.A. Moorman, D.W. Simonetti, S. Craig, D.R. Marshak, Multilineage potential of adult human mesenchymal stem cells, Science 284 (1999) 143–147.
[40] M. Doube, M.M. Klosowski, I. Arganda-Carreras, F.P. Cordelieres, R.P. Dougherty, J.S. Jackson, B. Schmid, J.R. Hutchinson, S.J. Shefelbine, BoneJ: Free and extensible bone image analysis in ImageJ, Bone 47 (2010) 1076–1079.
[41] J. Schindelin, I. Arganda-Carreras, E. Frise, V. Kaynig, M. Longair, T. Pietzsch, S. Preibisch, C. Rueden, S. Saalfeld, B. Schmid, J.Y. Tinevez, D.J. White, V. Hartenstein, K. Eliceiri, P. Tomancak, A. Cardona, Fiji: an open-source platform for biological-image analysis, Nat. Methods 9 (2012) 676–682.
[42] T.K. Koo, M.Y. Li, A guideline of selecting and reporting intraclass correlation coefficients for reliability research, J. Chiropr. Med. 15 (2016) 155–163.
[43] R.E. Guldberg, C.L. Duvall, A. Peister, M.E. Oest, A.S. Lin, A.W. Palmer, M.E. Levenston, 3D imaging of tissue integration with porous biomaterials, Biomaterials 29 (2008) 3757–3761.
[44] E. Frohlich, The role of surface charge in cellular uptake and cytotoxicity of medical nanoparticles, Int. J. Nanomed. 7 (2012) 5577–5591.
[45] M. Mashiatulla, M.M. Moran, D. Chan, J. Li, J.D. Freedman, B.D. Snyder, M.W. Grinstaff, A. Plaas, D.R. Sumner, Murine articular cartilage morphology and compositional quantification with high resolution cationic contrast-enhanced muCT, J. Orth. Res. 35 (2017) 2740–2748.
[46] M.S. Rachel, C. Stewart, P. Prashant, N. Bansal, M.D. Vahid Entezari, P. Hrvoje Lusic, M.D. Rosalynn, M. Nazarian, M.D.P. Brian, D. Snyder, P. Mark, W. Grinstaff, Contrast-enhanced CT with a high-affinity cationic contrast agent for imaging ex vivo bovine, intact ex vivo rabbit, and in vivo rabbit cartilage, Radiology 266 (2013) 141–150.
[47] T. Takahashi, H. Mizobuchi, M. Toda, A. Maeda, S. Mizuno, Y. Ogawa, S. Yoshida, H. Yamamoto, Metabolic effects of X-ray irradiation on adult human articular chondrocytes, Int. J. Mol. Med. 11 (2003) 631–634.
[48] B.S. Margulies, J.A. Horton, Y. Wang, T.A. Damron, M.J. Allen, Effects of radiation therapy on chondrocytes in vitro, Calcif. Tissue Int. 78 (2006) 302–313.
[49] Y. Saintigny, S. Cruet-Hennequart, D.H. Hamdi, F. Chevalier, J.L. Lefaix, Impact of therapeutic irradiation on healthy articular cartilage, Radiat. Res. 183 (2015) 135–146.
[50] T. Matsumoto, K. Iwasaki, H. Sugihara, Effects of radiation on chondrocytes in culture, Bone 15 (1994) 97–100.
[51] S. Cruet-Hennequart, C. Drougard, G. Shaw, F. Legendre, M. Demoor, F. Barry, J.L. Lefaix, P. Galera, Radiation-induced alterations of osteogenic and chondrogenic differentiation of human mesenchymal stem cells, PLoS One 10 (2015) e0119334.
[52] A. Jackson, W. Gu, Transport properties of cartilaginous tissues, Curr. Rheumatol. Rev. 5 (2009) 40–50.
[53] K.A. Kulmala, R.K. Korhonen, P. Julkunen, J.S. Jurvelin, T.M. Quinn, H. Kroger, J. Toyras, Diffusion coefficients of articular cartilage for different CT and MRI contrast agents, Med. Eng. Phys. 32 (2010) 878–882.
[54] A.G. Bajpayee, C.R. Wong, M.G. Bawendi, E.H. Frank, A.J. Grodzinsky, Avidin as a model for charge driven transport into cartilage and drug delivery for treating early stage post-traumatic osteoarthritis, Biomaterials 35 (2014) 538–549.
[55] A.G. Bajpayee, M. Scheu, A.J. Grodzinsky, R.M. Porter, A rabbit model demonstrates the influence of cartilage thickness on intra-articular drug delivery and retention within cartilage, J. Orth. Res. 33 (2015) 660–667.
[56] B. Pouran, V. Arbabi, A.G. Bajpayee, J. van Tiel, J. Toyras, J.S. Jurvelin, J. Malda, A.A. Zadpoor, H. Weinans, Multi-scale imaging techniques to investigate solute transport across articular cartilage, J. Biomech. 78 (2018) 10–20.
[57] C.E. Ghezzi, J. Rnjak-Kovacina, D.L. Kaplan, Corneal tissue engineering: recent advances and future perspectives, Tissue Eng. Part B Rev. 21 (2015) 278–287.
[58] E. Pacella, F. Pacella, G. De Paolis, F.R. Parisella, P. Turchetti, G. Anello, C. Cavallotti, Glycosaminoglycans in the human cornea: age-related changes, Ophthalmol. Eye Dis. 7 (2015) 1–5.
[59] M.A. Adams, P.J. Roughley, What is intervertebral disc degeneration, and what causes it? Spine (Phila Pa 1976) 31 (2006) 2151–2161.
[60] R. Kandel, S. Roberts, J.P. Urban, Tissue engineering and the intervertebral disc: the challenges, Eur. Spine J. 17 (Suppl 4) (2008) 480–491.
[61] E.H. Stephens, C.K. Chu, K.J. Grande-Allen, Valve proteoglycan content and glycosaminoglycan fine structure are unique to microstructure, mechanical load and age: Relevance to an age-specific tissue-engineered heart valve, Acta Biomater. 4 (2008) 1148–1160.
[62] M.S. Sacks, F.J. Schoen, J.E. Mayer, Bioengineering challenges for heart valve tissue engineering, Annu. Rev. Biomed. Eng. 11 (2009) 289–313.